JMEPEG (2012) 21:777–785
DOI: 10.1007/s11665-011-9968-2
©ASM International
1059-9495/$19.00

Case-Study Inverse Thermal Analyses of Al2139 Laser Welds

A.D. Zervaki, G.N. Haidemenopoulos, D.P. Vriami, and S.G. Lambrakos

(Submitted March 23, 2011)

Case study inverse thermal analyses of A12139 laser welds are presented. These analyses employ a numerical methodology that is in terms of analytic and numerical basis functions for inverse thermal analysis of steady state energy deposition in plate structures. The results of the case studies presented provide parametric representations of weld temperature histories that can be adopted as input data to various types of computational procedures, such as those for prediction of solid-state phase transformations and their associated software implementations. In addition, these weld temperature histories will be useful for construction of numerical basis functions that can be adopted for inverse analysis of welds corresponding to other process parameters or welding processes whose process conditions are within similar regimes.

Keywords aluminum, modeling processes, welding

1. Introduction

Case study inverse thermal analyses of A12139 laser welds are presented. These analyses provide a parameterization of temperature histories for prediction of properties within the heat affected zone (HAZ) of welds for the regime considered. These analyses employ a procedure that is in terms of analytic and numerical basis functions for steady-state energy deposition in plate structures. The formal structure of the numerical methodology underlying this procedure follows from a specific definition of the inverse heat-transfer problem, which is well posed for inverse analysis of heat-deposition processes. This definition is based on the assumption of the availability of information concerning spatially distributed boundary and constraint values. The results of the case study presented provide parametric representations of weld temperature histories that can be adopted as input data to various types of computational procedures, such as those for prediction of solid-state phase transformations and their associated software implementations. In addition, these weld temperature histories will be useful for construction of numerical basis functions that can be adopted for inverse analysis of welds corresponding to other process parameters or of welding processes process conditions of which are within similar regimes. The construction of temperature fields according to spatially and temporally distributed constraint conditions using linear combinations of optimal basis functions represents a highly convenient approach to the inverse analysis of energy-deposition processes. Basis functions can be terms of either analytic or numerical function representations, or both in linear combination.

The organization of the subject areas presented here are as follows. First, a brief description of the general procedure for inverse analysis of heat deposition processes is presented. Second, a description of the experimental procedure for generation of laser welds of the Aluminum alloy A12139 is presented. Third, results of inverse thermal analyses of A12139 laser welds are presented. These results provide a quantitative parametric representation of temperature histories for these welds and for any welds associated with similar weld process conditions. Finally, a conclusion is given.

A.D. Zervaki, G.N. Haidemenopoulos, and **D.P. Vriami**, Department of Mechanical Engineering, University of Thessaly, 38334 Volos, Greece; and **S.G. Lambrakos**, Center for Computational Materials, Code 6390, Materials Science and Technology Division, Naval Research Laboratory, Washington, DC. Contact e-mail: lambrakos@anvil.nrl.navy.mil.

2. Inverse Analysis Procedure

Following the inverse analysis approach (Ref 1-5), a parametric representation based on a physical model provides a means for the inclusion of information concerning the physical characteristics of a given energy deposition process. It follows then that for heat deposition processes involving the deposition of heat within a bounded region of finite volume, consistent parametric representations of the temperature field are given by

$$T(\hat{x},t) = T_{\mathrm{A}} + \sum_{k=1}^{N_k} w_k T_k(\hat{x},\hat{x}_k,\kappa,t) \quad \text{and} \quad T(\hat{x}_n^{\mathrm{c}},t_n^{\mathrm{c}}) = T_n^{\mathrm{c}} \tag{Eq 1}$$

where $T_k(\hat{x},\hat{x}_k,\kappa,t)$ represent an effectively complete set of basis functions for representation of the temperature field within the region bounded by surfaces S_{i} and S_{o}. The quantity T_{A} is the ambient temperature of the workpiece and the locations $\hat{x}_n^{\mathrm{c}}$, and temperature values T_n^{c} specify constraint conditions on the temperature field. The functions $T_k(\hat{x},\hat{x}_k,\kappa,t)$ represent an optimal basis set of functions for given sets of boundary conditions and material properties.

The quantities $\hat{x}_k = (x_k, y_k, z_k)$, $k = 1, \ldots, N_k$, are the locations of the elemental source or boundary elements. The sum defined by Eq 2 can for certain systems specify numerical integration over the discrete elements of a distribution of sources or boundary elements. Selection of an optimal set of basis functions is based on a consideration of the characteristic model and data spaces of heat deposition processes and subsequently isolating those regions of the model space corresponding to parameterizations that are both physically consistent and sufficiently general in terms of their mathematical representation and mapping from data to model space. Although heat deposition processes may be characterized by complex coupling between the heat source and workpiece, as well as complex geometries associated with either the workpiece or deposition process, in terms of inverse analysis the general functional forms of the temperature fields associated with all such processes are within a restricted class of functions, i.e., optimal sets of functions. Accordingly, sufficiently optimal set of functions contains the analytic solutions to heat conduction equation for a finite set of boundary conditions. A parameterization based on this set is both sufficiently general and convenient relative to optimization.

The formal procedure underlying the inverse method considered in this article entails the adjustment of the temperature field defined over the entire spatial region of the sample volume at a given time t. This approach defines an optimization procedure where the temperature field spanning the spatial region of the sample volume is adopted as the quantity to be optimized. The constraint conditions are imposed on the temperature field spanning the bounded spatial domain of the workpiece by minimization of the value of the objective functions defined by

$$Z_{\mathrm{T}} = \sum_{n=1}^{N} w_n \left(T(\hat{x}_n^{\mathrm{c}}, t_n^{\mathrm{c}}) - T_n^{\mathrm{c}} \right)^2 \qquad \text{(Eq 2)}$$

where T_n^{c} is the target temperature for position $\hat{x}_n^{\mathrm{c}} = (x_n^{\mathrm{c}}, y_n^{\mathrm{c}}, z_n^{\mathrm{c}})$ and w_n is a weighting coefficient.

The input of information into the inverse model defined by Eq 1 and 2, i.e., the mapping from data to model space, is effected by the assignment of individual constraint values to the quantities T_n^{c}; the form of the basis functions adopted for parametric representation; and specifying the shapes of the inner and outer boundaries, S_{i} and S_{o}, respectively, which bound the temperature field within a specified region of the workpiece. The constraint conditions and basis functions, i.e., $T(\hat{x}_n^{\mathrm{c}}, t_n^{\mathrm{c}}) = T_n^{\mathrm{c}}$ and $T_k(\hat{x}, \hat{x}_k, \kappa, t)$, respectively, provide for the inclusion of information that can be obtained from both laboratory and numerical experiments.

Within the context of the numerical method presented, a set of basis functions is considered effectively complete if these functions provided reasonably optimal fitting to boundary and constraint conditions. Before proceeding, it is significant to note that, in principle, the set of basis functions adopted by Eq 1 can be defined in terms of either analytic or numerical

Table 1 Chemical composition of Al2139-T3 (wt.%)

Si	Fe	Cu	Mn	Mg	Cr	Zn	Zr	Li	Ag	Ti
0.04	0.06	4.79	0.3	0.45	…	<0.01	0.01	…	0.34	0.05

Table 2 Temperature field constraint conditions at positions (y_c, z_c) on transverse cross sections of welds at solidification boundaries

Power P	3630 W	3818 W	3630 W	3724 W	3818 W	3818 W	3724 W	3630 W	3441 W	3535 W	3535 W	3535 W	3724 W	3724 W	3771 W
Speed V	2 m/min	2 m/min	1.6 m/min	1.6 m/min	1.6 m/min	1.8 m/min	1.83 m/min	1.83 m/min	1.6 m/min	1.6 m/min	1.6 m/min	1.6 m/min	1.6 m/min	1.6 m/min	1.6 m/min
Input h	109 J/mm	115 J/mm	136 J/mm	140 J/mm	143 J/mm	127 J/mm	122 J/mm	119 J/mm	129 J/mm	133 J/mm	133 J/mm	133 J/mm	140 J/mm	140 J/mm	141 J/mm
Focal Point	0 mm	0 mm	0 mm	0.5 mm	0 mm	0 mm	0 mm	0 mm	0 mm	0 mm	0.5 mm	0.5 mm	0 mm	0 mm	0 mm
z_c, mm	$2y_c$, mm	$2y_c$, mm	$2y_c$, mm	$2y_c$, mm	$2y_c$, mm	$2y_c$, mm	$2y_c$, mm	$2y_c$, mm	$2y_c$, mm	$2y_c$, mm	$2y_c$, mm	$2y_c$, mm	$2y_c$, mm	$2y_c$, mm	$2y_c$, mm
0.0	4.0	4.4	4.9	4.8	5.0	4.6	4.5	4.4	4.5	4.3	4.2	4.8	4.7	5.0	4.6
0.5	3.9	4.2	4.7	4.8	4.7	4.3	4.4	4.1	4.3	4.2	4.5	4.5	4.5	5.0	4.5
1.0	2.9	3.5	3.8	4.3	4.3	3.6	3.7	3.5	3.7	3.6	4.0	3.3	3.4	4.5	3.8
1.5	2.4	2.5	2.7	3.3	3.4	2.8	3.1	2.7	3.0	3.0	3.3	2.7	2.7	3.3	2.8
2.0	2.2	2.3	2.5	2.7	2.7	2.5	2.6	2.4	2.5	2.4	2.6	2.4	2.6	2.6	2.5
2.5	1.8	2.1	2.3	2.3	2.5	2.4	2.4	2.3	2.4	2.4	2.4	2.2	2.5	2.5	2.4
3.0	1.4	1.7	2.1	2.0	2.3	2.3	2.3	2.1	2.1	2.2	2.2	2.0	2.0	2.3	2.3
3.5	0.0	1.3	1.7	1.7	2.0	2.0	2.1	1.7	2.0	1.8	1.9	1.6	2.0	2.0	1.9
4.0		0.0	1.0	1.2	2.5	1.8	1.9	1.2	1.6	1.5	1.5	1.3	1.9	1.9	1.4
4.3			0.0	0.0											
4.4												0.0			
4.5					1.6	1.7	1.7	0.0	1.3	1.3	1.2		1.8	1.1	
Figure	1	2	3	4	5(a)	5(b)	5(c)	5(d)	5(e)	5(f)	5(g)	5(h)	5(i)	5(j)	

Table 3 Volumetric source function $C(\hat{x}_k)$ calculated according to constraint conditions specified by weld cross sections shown in Fig. 1, where Δl = 4.5/60 mm

k	$C(\hat{x}_k)$/1.3	$x_k(\Delta l)$	$y_k(\Delta l)$	$z_k(\Delta l)$
1	0.09	0.0	0.0	3.0
2	0.085	0.0	0.0	5.0
3	0.08	0.0	0.0	7.0
4	0.08	0.0	0.0	9.0
5	0.1	4.0	0.0	0.0
6	0.1	−4.0	0.0	0.0
	$C(\hat{x}_k)$/0.5	$x_k(\Delta l)$	$y_k(\Delta l)$	$z_k(\Delta l)$
7	0.1	0.0	4.0	0.0
8	0.1	0.0	−4.0	0.0

Table 4 Volumetric source function $C(\hat{x}_k)$ calculated according to constraint conditions specified by weld cross sections shown in Fig. 2, where Δl = 4.5/60 mm

k	$C(\hat{x}_k)$/1.5	$x_k(\Delta l)$	$y_k(\Delta l)$	$z_k(\Delta l)$
1	0.09	0.0	0.0	3.0
2	0.085	0.0	0.0	5.0
3	0.08	0.0	0.0	7.0
4	0.095	0.0	0.0	9.0
5	0.005	0.0	0.0	10.0
	$C(\hat{x}_k)$/1.3	$x_k(\Delta l)$	$y_k(\Delta l)$	$z_k(\Delta l)$
6	0.1	4.0	0.0	0.0
7	0.1	−4.0	0.0	0.0
	$C(\hat{x}_k)$/0.7	$x_k(\Delta l)$	$y_k(\Delta l)$	$z_k(\Delta l)$
8	0.1	0.0	4.0	0.0
9	0.1	0.0	−4.0	0.0

Table 5 Volumetric source function $C(\hat{x}_k)$ calculated according to constraint conditions specified by weld cross sections shown in Fig. 3, where Δl = 4.5/60 mm

k	$C(\hat{x}_k)$/1.5	$x_k(\Delta l)$	$y_k(\Delta l)$	$z_k(\Delta l)$
1	0.09	0.0	0.0	3.0
2	0.085	0.0	0.0	5.0
3	0.08	0.0	0.0	7.0
4	0.095	0.0	0.0	9.0
5	0.04	0.0	0.0	11.0
	$C(\hat{x}_k)$/1.3	$x_k(\Delta l)$	$y_k(\Delta l)$	$z_k(\Delta l)$
6	0.1	4.0	0.0	0.0
7	0.1	−4.0	0.0	0.0
	$C(\hat{x}_k)$/1.0	$x_k(\Delta l)$	$y_k(\Delta l)$	$z_k(\Delta l)$
8	0.1	0.0	4.0	0.0
9	0.1	0.0	−4.0	0.0

function representations. The numerical method that is developed for this study employs both analytic and numerical function representations of basis function adopted for the

Table 6 Volumetric source function $C(\hat{x}_k)$ calculated according to constraint conditions specified by weld cross sections shown in Fig. 4, where Δl = 4.5/60 mm

k	$C(\hat{x}_k)$/1.4	$x_k(\Delta l)$	$y_k(\Delta l)$	$z_k(\Delta l)$
1	0.09	0.0	0.0	3.0
2	0.085	0.0	0.0	5.0
3	0.08	0.0	0.0	7.0
4	0.095	0.0	0.0	9.0
5	0.055	0.0	0.0	11.0
	$C(\hat{x}_k)$/1.5	$x_k(\Delta l)$	$y_k(\Delta l)$	z_k ($y\Delta l$)
6	0.1	4.0	0.0	0.0
	$C(\hat{x}_k)$/1.3	$x_k(\Delta l)$	$y_k(\Delta l)$	$z_k(\Delta l)$
7	0.1	−4.0	0.0	0.0
	$C(\hat{x}_k)$/1.25	$x_k(\Delta l)$	$y_k(\Delta l)$	$z_k(\Delta l)$
8	0.1	0.0	4.0	0.0
9	0.1	0.0	−4.0	0.0

Table 7 Volumetric source function $C(\hat{x}_k)$ calculated according to constraint conditions specified by weld cross sections shown in Fig. 5(a), where Δl = 4.5/60 mm

k	$C(\hat{x}_k)$/1.5	$x_k(\Delta l)$	$y_k(\Delta l)$	$z_k(\Delta l)$
1	0.09	0.0	0.0	3.0
2	0.085	0.0	0.0	5.0
3	0.08	0.0	0.0	7.0
4	0.095	0.0	0.0	9.0
5	0.06	0.0	0.0	11.0
6	0.015	0.0	0.0	13.0
	$C(\hat{x}_k)$/1.3	$x_k(\Delta l)$	$y_k(\Delta l)$	$z_k(\Delta l)$
7	0.1	4.0	0.0	0.0
8	0.1	−4.0	0.0	0.0
	$C(\hat{x}_k)$/1.2	$x_k(\Delta l)$	$y_k(\Delta l)$	$z_k(\Delta l)$
9	0.1	0.0	4.0	0.0
10	0.1	0.0	−4.0	0.0

calculation of temperature fields within bounded domains within which constraint conditions are specified. In addition, the interrelation between analytic and numerical basis function representations is an important aspect of the numerical method. Next, a consistent representation Eq 1 of the temperature field for heat deposition within structures characterized by a finite thickness, in terms of analytic basis functions, i.e., analytic solutions to the heat conduction equation (Ref 6), is

$$T(\hat{x},t) = T_{\mathrm{A}} + \sum_{k=1}^{N_k}\sum_{n=1}^{N_t} C(\hat{x}_k)G(\hat{x},\hat{x}_k,\kappa,n\Delta t,V) \quad T(\hat{x}_n^{\mathrm{c}},t_n^{\mathrm{c}}) = T_n^{\mathrm{c}} \tag{Eq 3}$$

where

Table 8 Volumetric source function $C(\hat{x}_k)$ calculated according to constraint conditions specified by weld cross sections shown in Fig. 5(b), where Δl = 4.5/60 mm

k	$C(\hat{x}_k)$/1.5	$x_k(\Delta l)$	$y_k(\Delta l)$	$z_k(\Delta l)$
1	0.09	0.0	0.0	3.0
2	0.085	0.0	0.0	5.0
3	0.08	0.0	0.0	7.0
4	0.095	0.0	0.0	9.0
5	0.06	0.0	0.0	11.0
6	0.017	0.0	0.0	13.0
	$C(\hat{x}_k)$/1.3	$x_k(\Delta l)$	$y_k(\Delta l)$	$z_k(\Delta l)$
7	0.1	4.0	0.0	0.0
8	0.1	−4.0	0.0	0.0
	$C(\hat{x}_k)$/0.85	$x_k(\Delta l)$	$y_k(\Delta l)$	$z_k(\Delta l)$
9	0.1	0.0	4.0	0.0
10	0.1	0.0	−4.0	0.0

Table 9 Volumetric source function $C(\hat{x}_k)$ calculated according to constraint conditions specified by weld cross sections shown in Fig. 5(c), where Δl = 4.5/60 mm

k	$C(\hat{x}_k)$/1.5	$x_k(\Delta l)$	$y_k(\Delta l)$	$z_k(\Delta l)$
1	0.09	0.0	0.0	3.0
2	0.085	0.0	0.0	5.0
3	0.08	0.0	0.0	7.0
4	0.095	0.0	0.0	9.0
5	0.06	0.0	0.0	11.0
6	0.017	0.0	0.0	13.0
7	0.1	4.0	0.0	0.0
	$C(\hat{x}_k)$/1.3	$x_k(\Delta l)$	$y_k(\Delta l)$	$z_k(\Delta l)$
8	0.1	−4.0	0.0	0.0
	$C(\hat{x}_k)$/0.85	$x_k(\Delta l)$	$y_k(\Delta l)$	$z_k(\Delta l)$
9	0.1	0.0	4.0	0.0
10	0.1	0.0	−4.0	0.0

$$G(\hat{x},\hat{x}_k,t,\kappa,V) = \frac{1}{t}\exp\left[-\frac{(x-x_k-Vt)^2+(y-y_k)^2}{4\kappa t}\right] \times\left\{1+2\sum_{m=1}^{\infty}\exp\left[-\frac{\kappa m^2\pi^2 t}{l^2}\right]\cos\left[\frac{m\pi z}{l}\right]\cos\left[\frac{m\pi z_k}{l}\right]\right\}, \quad \text{(Eq 4)}$$

and

$$C(\hat{x}) = \sum_{k=1}^{N_k} Q(\hat{x}_k)\delta(\hat{x}-\hat{x}_k). \quad \text{(Eq 5)}$$

The quantities κ, V and l are the thermal diffusivity, welding speed, and plate thickness, respectively. The procedure for inverse analysis defined by Eq 2-5 entails adjustment of the

Table 10 Volumetric source function $C(\hat{x}_k)$ calculated according to constraint conditions specified by weld cross sections shown in Fig. 5(d), where Δl = 4.5/60 mm

k	$C(\hat{x}_k)$/1.5	$x_k(\Delta l)$	$y_k(\Delta l)$	$z_k(\Delta l)$
1	0.09	0.0	0.0	3.0
2	0.085	0.0	0.0	5.0
3	0.08	0.0	0.0	7.0
4	0.095	0.0	0.0	9.0
5	0.05	0.0	0.0	11.0
6	0.1	4.0	0.0	0.0
	$C(\hat{x}_k)$/1.3	$x_k(\Delta l)$	$y_k(\Delta l)$	$z_k(\Delta l)$
7	0.1	−4.0	0.0	0.0
	$C(\hat{x}_k)$/0.7	$x_k(\Delta l)$	$y_k(\Delta l)$	$z_k(\Delta l)$
8	0.1	0.0	4.0	0.0
9	0.1	0.0	−4.0	0.0

Table 11 Volumetric source function $C(\hat{x}_k)$ calculated according to constraint conditions specified by weld cross sections shown in Fig. 5(e), where Δl = 4.5/60 mm

k	$C(\hat{x}_k)$/1.5	$x_k(\Delta l)$	$y_k(\Delta l)$	$z_k(\Delta l)$
1	0.09	0.0	0.0	3.0
2	0.085	0.0	0.0	5.0
3	0.08	0.0	0.0	7.0
4	0.095	0.0	0.0	9.0
5	0.05	0.0	0.0	11.0
6	0.01	0.0	0.0	13.0
7	0.1	4.0	0.0	0.0
	$C(\hat{x}_k)$/1.3	$x_k(\Delta l)$	$y_k(\Delta l)$	$z_k(\Delta l)$
8	0.1	−4.0	0.0	0.0
	$C(\hat{x}_k)$/0.7	$x_k(\Delta l)$	$y_k(\Delta l)$	$z_k(\Delta l)$
9	0.1	0.0	4.0	0.0
10	0.1	0.0	−4.0	0.0

Table 12 Volumetric source function $C(\hat{x}_k)$ calculated according to constraint conditions specified by weld cross sections shown in Fig. 5(f), where Δl = 4.5/60 mm

k	$C(\hat{x}_k)$/1.5	$x_k(\Delta l)$	$y_k(\Delta l)$	$z_k(\Delta l)$
1	0.09	0.0	0.0	3.0
2	0.085	0.0	0.0	5.0
3	0.08	0.0	0.0	7.0
4	0.095	0.0	0.0	9.0
5	0.05	0.0	0.0	11.0
6	0.01	0.0	0.0	13.0
7	0.1	4.0	0.0	0.0
	$C(\hat{x}_k)$/1.3	$x_k(\Delta l)$	$y_k(\Delta l)$	$z_k(\Delta l)$
8	0.1	−4.0	0.0	0.0
	$C(\hat{x}_k)$/0.67	$x_k(\Delta l)$	$y_k(\Delta l)$	$z_k(\Delta l)$
9	0.1	0.0	4.0	0.0
10	0.1	0.0	−4.0	0.0

Table 13 Volumetric source function $C(\hat{x}_k)$ calculated according to constraint conditions specified by weld cross sections shown in Fig. 5(g), where Δl = 4.5/60 mm

k	$C(\hat{x}_k)$/1.5	$x_k(\Delta l)$	$y_k(\Delta l)$	$z_k(\Delta l)$
1	0.09	0.0	0.0	3.0
2	0.085	0.0	0.0	5.0
3	0.08	0.0	0.0	7.0
4	0.095	0.0	0.0	9.0
5	0.06	0.0	0.0	11.0
6	0.01	0.0	0.0	13.0
7	0.1	4.0	0.0	0.0
	$C(\hat{x}_k)$/1.3	$x_k(\Delta l)$	$y_k(\Delta l)$	$z_k(\Delta l)$
8	0.1	−4.0	0.0	0.0
	$C(\hat{x}_k)$/1.0	$x_k(\Delta l)$	$y_k(\Delta l)$	$z_k(\Delta l)$
9	0.1	0.0	4.0	0.0
10	0.1	0.0	−4.0	0.0

Table 14 Volumetric source function $C(\hat{x}_k)$ calculated according to constraint conditions specified by weld cross sections shown in Fig. 5(h), where Δl = 4.5/60 mm

k	$C(\hat{x}_k)$/1.3	$x_k(\Delta l)$	$y_k(\Delta l)$	$z_k(\Delta l)$
1	0.09	0.0	0.0	3.0
2	0.085	0.0	0.0	5.0
3	0.08	0.0	0.0	7.0
4	0.095	0.0	0.0	9.0
5	0.063	0.0	0.0	11.0
	$C(\hat{x}_k)$/1.5	$x_k(\Delta l)$	$y_k(\Delta l)$	$z_k(\Delta l)$
6	0.1	4.0	0.0	0.0
	$C(\hat{x}_k)$/1.3	$x_k(\Delta l)$	$y_k(\Delta l)$	$z_k(\Delta l)$
7	0.1	−4.0	0.0	0.0
	$C(\hat{x}_k)$/0.95	$x_k(\Delta l)$	$y_k(\Delta l)$	$z_k(\Delta l)$
8	0.1	0.0	4.0	0.0
9	0.1	0.0	−4.0	0.0

parameters $C(\hat{x}_k)$, $\hat{x}_k$ and Δt defined over the entire spatial region of the workpiece.

3. Experimental Procedure

The heat-treatable Aluminum alloy used for this study is the Al-alloy 2139-T3, with plate dimension 100 × 100 × 4.5 mm, respectively. Chemical composition of this alloy (in wt.%) is given in Table 1.

A Trumpf TLF 12000 CO_2 laser was employed for the welding experiments. The lens of the welding head had a focal distance of 171.5 mm, and the beam spot size at the focal point position was 0.6 mm. Shielding gas (50:50 mixture of Ar and He) was supplied coaxially to the laser beam for plasma suppression during keyhole formation to avoid loss of alloying elements, especially magnesium, from vaporization.

Table 15 Volumetric source function $C(\hat{x}_k)$ calculated according to constraint conditions specified by weld cross sections shown in Fig. 5(i), where Δl = 4.5/60 mm

k	$C(\hat{x}_k)$/1.5	$x_k(\Delta l)$	$y_k(\Delta l)$	$z_k(\Delta l)$
1	0.09	0.0	0.0	3.0
2	0.085	0.0	0.0	5.0
3	0.08	0.0	0.0	7.0
4	0.095	0.0	0.0	9.0
5	0.063	0.0	0.0	11.0
6	0.02	0.0	0.0	13.0
7	0.1	4.0	0.0	0.0
	$C(\hat{x}_k)$/1.3	$x_k(\Delta l)$	$y_k(\Delta l)$	$z_k(\Delta l)$
8	0.1	−4.0	0.0	0.0
	$C(\hat{x}_k)$/1.37	$x_k(\Delta l)$	$y_k(\Delta l)$	$z_k(\Delta l)$
9	0.1	0.0	4.0	0.0
10	0.1	0.0	−4.0	0.0

Table 16 Volumetric source function $C(\hat{x}_k)$ calculated according to constraint conditions specified by weld cross sections shown in Fig. 5(j), where Δl = 4.5/60 mm

k	$C(\hat{x}_k)$/1.5	$x_k(\Delta l)$	$y_k(\Delta l)$	$z_k(\Delta l)$
1	0.09	0.0	0.0	3.0
2	0.085	0.0	0.0	5.0
3	0.08	0.0	0.0	7.0
4	0.095	0.0	0.0	9.0
5	0.063	0.0	0.0	11.0
6	0.005	0.0	0.0	13.0
7	0.1	4.0	0.0	0.0
	$C(\hat{x}_k)$/1.3	$x_k(\Delta l)$	$y_k(\Delta l)$	$z_k(\Delta l)$
8	0.1	−4.0	0.0	0.0
	$C(\hat{x}_k)$/0.9	$x_k(\Delta l)$	$y_k(\Delta l)$	$z_k(\Delta l)$
9	0.1	0.0	4.0	0.0
10	0.1	0.0	−4.0	0.0

Bead-on-plate experiments were conducted and the welding conditions, including laser travel speed and focal point position, are given in Table 2. In these tables, laser welding conditions of power P (W) and travel speed V (m/min) are represented by the heat input parameter (h) which is defined by $h = P/V$ (J/mm). Specimens for metallographic evaluation were cut from the welded plates in directions longitudinal and transverse to the weld direction. Standard metallographic specimen preparation was employed including grinding, polishing, and etching. The etchant for macrostructure was a mixture of HCl, HNO_3, HF, and H_2O. For revealing microstructure, Keller's reagent was used.

4. Case Study Analysis of Al2139 Laser Welds

As for previous case studies, the procedure for construction of numerical basis functions adopted here entails

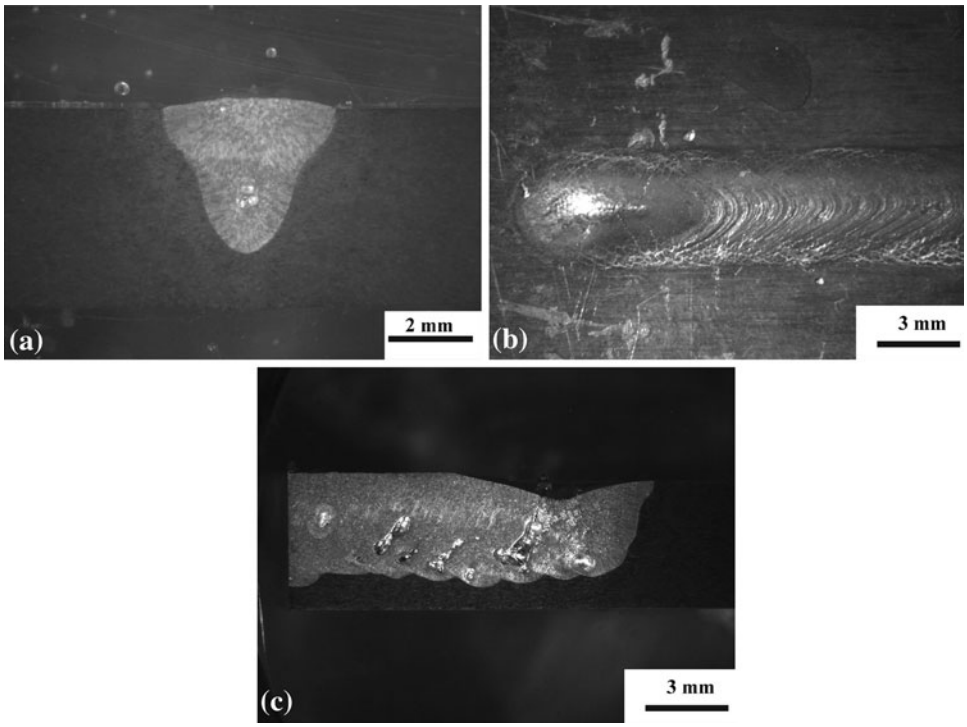

Fig. 1 Laser beam weld of Al2139-T3 for energy deposition of 109 J/mm and beam focal point at top surface of workpiece. (a) Transverse cross section. (b) Top surface of workpiece. (c) Longitudinal cross section at symmetry plane. Beam power and welding speed are 3630 W and 2 m/min, respectively

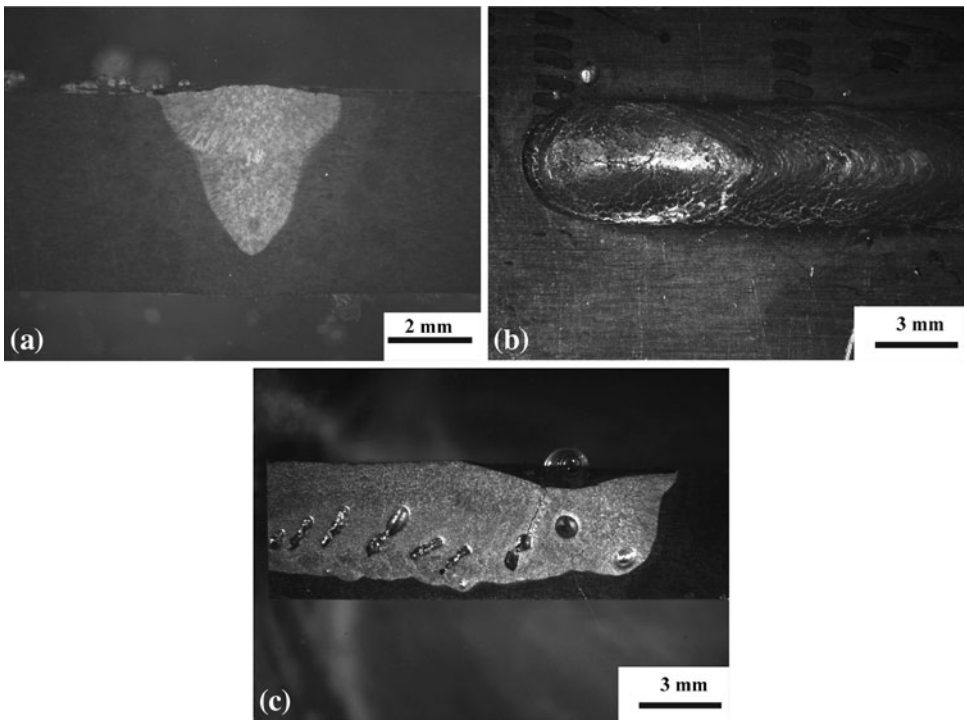

Fig. 2 Laser beam weld of Al2139-T3 for energy deposition of 115 J/mm and beam focal point at top surface of workpiece. (a) Transverse cross section. (b) Top surface of workpiece. (c) Longitudinal cross section at symmetry plane. Beam power and welding speed are 3818 W and 2 m/min, respectively

calculation of the steady state temperature field for a specified range of sizes and shapes of the inner surface boundary S_i defined by the solidification boundary for a range of welding process parameters. For this system, the parameter values assumed are $\kappa = 1.88 \times 10^{-5}$ m^2/s, $T_M = 548$°C (solidus temperature of 2139-T3 Aluminum), and $l = 4.5$ mm. The

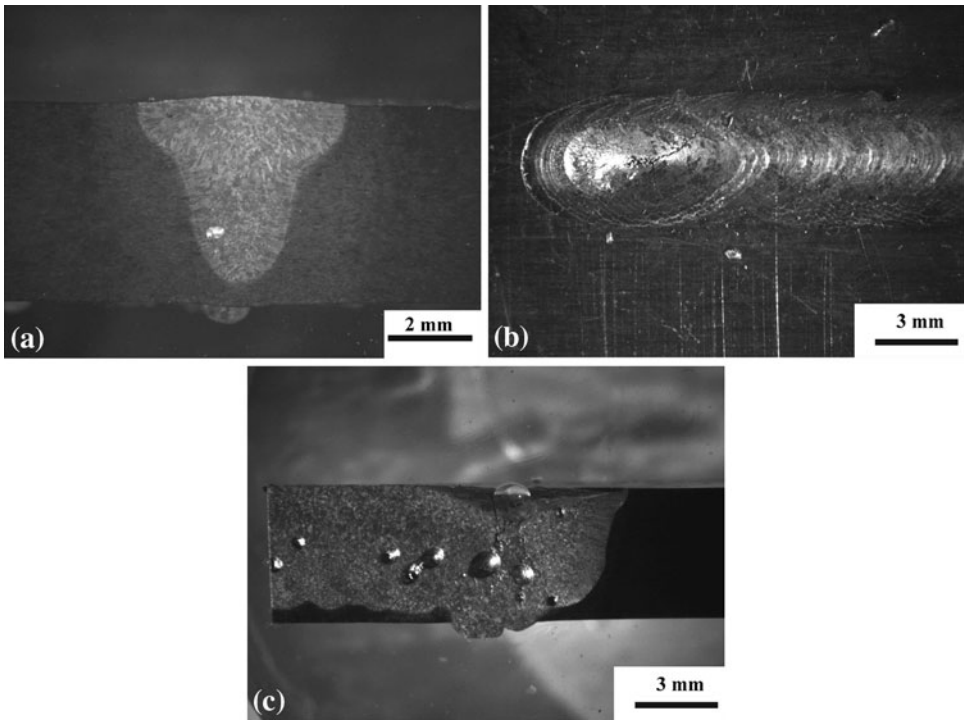

Fig. 3 Laser beam weld of Al2139-T3 for energy deposition of 136 J/mm and beam focal point at top surface of workpiece. (a) Transverse cross section. (b) Top surface of workpiece. (c) Longitudinal cross section at symmetry plane. Beam power and welding speed are 3630 W and 1.6 m/min, respectively

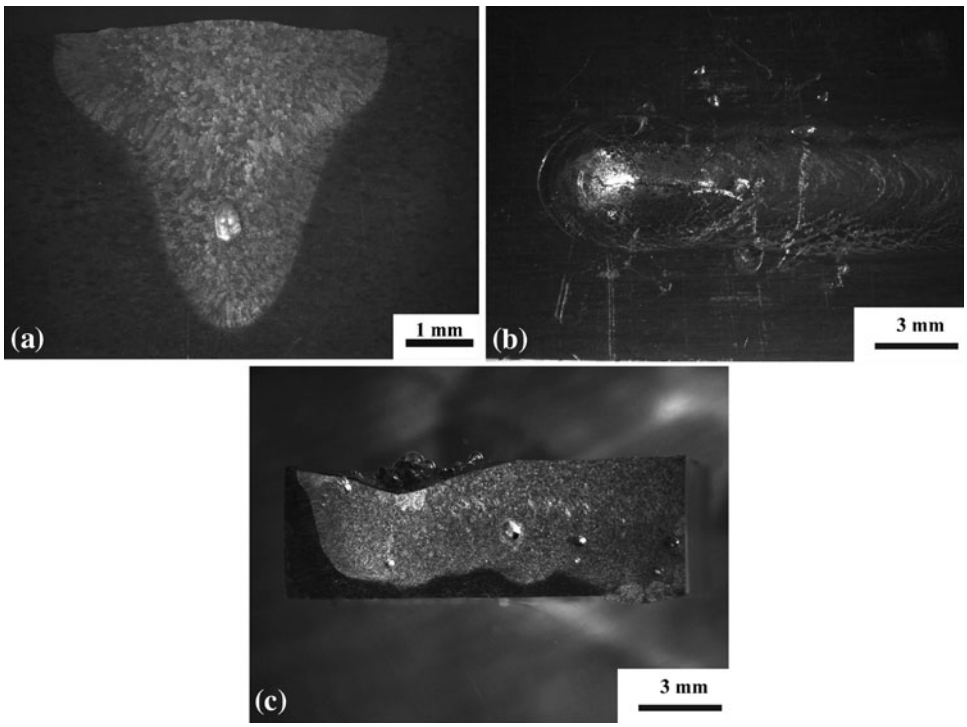

Fig. 4 Laser beam weld of Al2139-T3 for energy deposition of 140 J/mm and beam focal point at 0.5 mm above surface of workpiece. (a) Transverse cross section. (b) Top surface of workpiece. (c) Longitudinal cross section at symmetry plane. Beam power and welding speed are 3724 W and 1.6 m/min, respectively

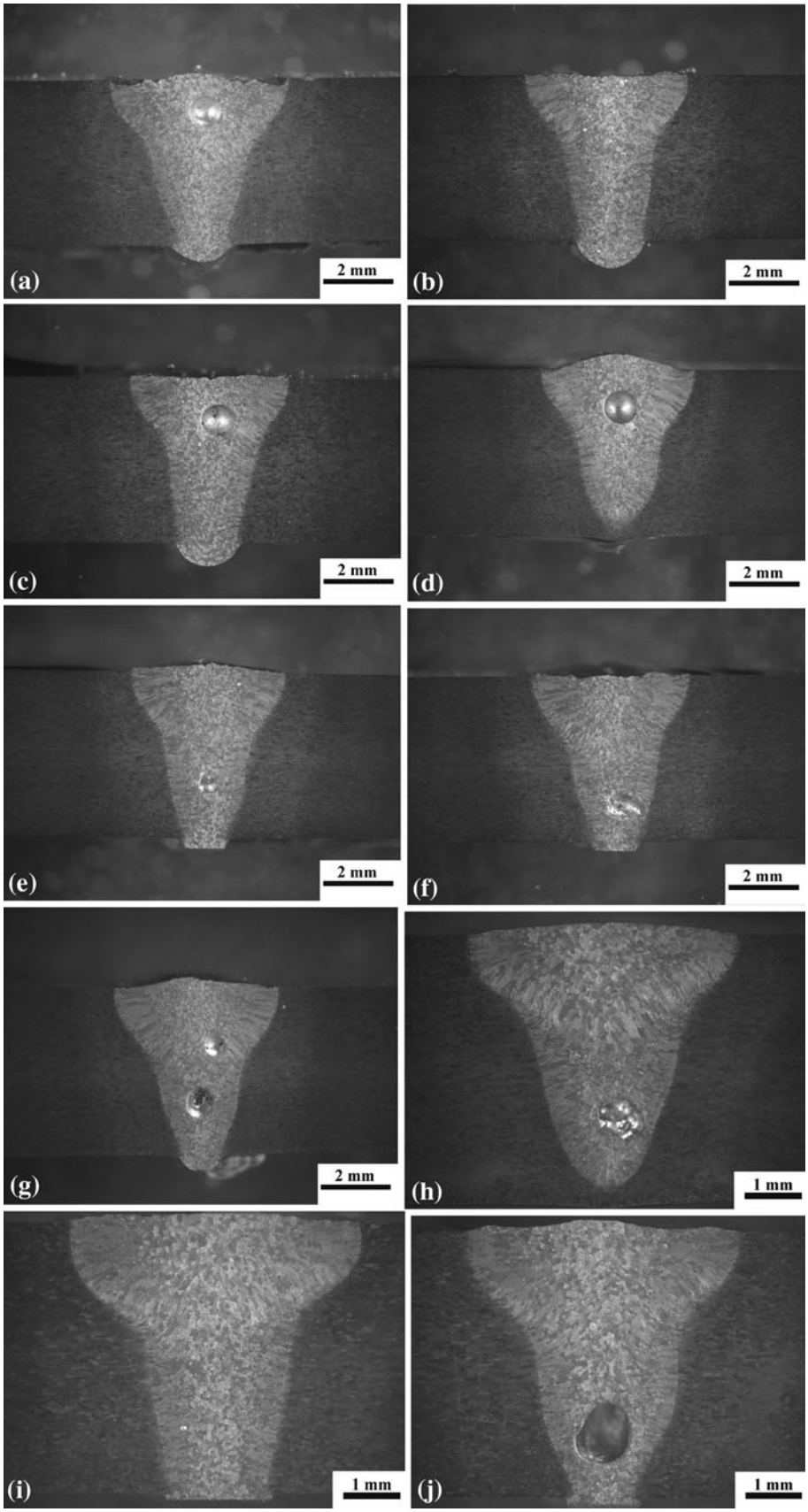

Fig. 5 Transverse cross sections of laser beam welds of Al2139-T3 corresponding to different process parameters (see Table 2)

upstream boundary constraints on the temperature field, $T_c = T_M$ for (y_c, z_c) defined in Eq 3, are given in Table 2. Given in Tables 3-16 are values of the discrete source function that have been calculated according to the constraint conditions and weld process parameters given in Table 2 (Fig. 1-5).

5. Conclusion

Tables 3-16 provide a parametric representation of the temperature field for the welding processes considered here in terms of linear combinations of numerical basis functions. That is to say, these tables specify a set of basis functions for representation of the temperature field for welding processes whose parameter values are within the associated neighborhood of parameter space. Accordingly, the procedure for calculation of temperature field values entails small adjustments of the coefficients A_k defined in the expression:

$$T(\hat{x}, t) = T_A + \sum_{k=1}^{N_k} \sum_{n=1}^{N_t} A_k C(\hat{x}_k) G(\hat{x}, \hat{x}_k, \kappa, n\Delta t), \qquad \text{(Eq 6)}$$

where $T(\hat{x}_n^c, t_n^c) = T_n^c$, values of the source function $C(\hat{x}_k)$ are given in Tables 3-16, and the function $G(\hat{x}, \hat{x}_k, \kappa, n\Delta t)$ is given by Eq 4. The objective of this report is to provide a set of parameters for a quantitative inverse thermal analysis of Al2139 laser welds corresponding to a specific range of weld process parameters and to construct numerical basis functions that can be used by weld analyst to calculated weld temperature histories, which are for welding processes associated with similar process conditions. In addition, the results that are presented in this report contribute to the continuing evolution of a multidimensional temperature field $T(\hat{x}, t, \kappa, V, l)$, which can be adopted for subsequent inverse thermal analysis by construction of numerical basis functions by interpolation within the (κ, V, l) parameter space.

Acknowledgments

The authors (ADZ and GNH) would like to thank the German Research Foundation DFG for the support of the depicted research within the Cluster of Excellence "Integrative Production Technology for High-Wage Countries" at RWTH Aachen University. Also ADZ acknowledges the support of Dr. Alexander Drenker of Fraunhofer-Institut für Lasertechnik during the experimental investigation. One of the authors (SGL) acknowledges the support provided by the Naval Research Laboratory (NRL) internal core program and active scientific collaboration with the University of Thessaly.

References

1. S.G. Lambrakos, A.D. Zervaki, G.N. Haidemenopoulos, and V. Stergiou, Basis Functions and Parameterizations for Inverse Analysis of Welding Processes, *Mathematical Modelling of Weld Phenomena*, Vol 9, Verlag der Technischen Universite Graz, Graz, 2011, p 793–815
2. A.D. Zervaki, G.N. Haidemenopoulos, and S.G. Lambrakos, Analysis of Heat Affected Zone Using Direct and Inverse Modelling in 6XXX Aluminum Alloys, *Mathematical Modelling of Weld Phenomena*, Vol 8, Verlag der Technischen Universite Graz, Graz, 2007, p 907–923
3. S.G. Lambrakos and S.G. Michopoulos, Algorithms for Inverse Analysis of Heat Deposition Processes, *Mathematical Modelling of Weld Phenomena*, Vol 8, Published by Verlag der Technischen Universite Graz, Graz, 2007, p 847–879
4. S.G. Lambrakos and J.O. Milewski, Analysis of Welding and Heat Deposition Processes Using an Inverse-Problem Approach, *Mathematical Modelling of Weld Phenomena*, Vol 7, Verlag der Technischen Universite Graz, Graz, 2005, p 1025–1055
5. J. Xie and J. Zou, Numerical Reconstruction of Heat Fluxes, *SIAM J. Numer. Anal.*, 2005, **43**(4), p 1504–1535
6. H.S. Carslaw and J.C. Jaegar, *Conduction of Heat in Solids*, 2nd ed., Clarendon Press, Oxford, 1959, p 374